LETTER

doi:10.1038/nature12205

Small molecule inhibition of the KRAS–PDEδ interaction impairs oncogenic KRAS signalling

Gunther Zimmermann[1]*, Björn Papke[2]*, Shehab Ismail[3]*, Nachiket Vartak[2], Anchal Chandra[2], Maike Hoffmann[4], Stephan A. Hahn[4], Gemma Triola[1], Alfred Wittinghofer[3], Philippe I. H. Bastiaens[2,5] & Herbert Waldmann[1,5]

The KRAS oncogene product is considered a major target in anticancer drug discovery[1–3]. However, direct interference with KRAS signalling has not yet led to clinically useful drugs[3–8]. Correct localization and signalling by farnesylated KRAS is regulated by the prenyl-binding protein PDEδ, which sustains the spatial organization of KRAS by facilitating its diffusion in the cytoplasm[9–11]. Here we report that interfering with binding of mammalian PDEδ to KRAS by means of small molecules provides a novel opportunity to suppress oncogenic RAS signalling by altering its localization to endomembranes. Biochemical screening and subsequent structure-based hit optimization yielded inhibitors of the KRAS–PDEδ interaction that selectively bind to the prenyl-binding pocket of PDEδ with nanomolar affinity, inhibit oncogenic RAS signalling and suppress *in vitro* and *in vivo* proliferation of human pancreatic ductal adenocarcinoma cells that are dependent on oncogenic KRAS. Our findings may inspire novel drug discovery efforts aimed at the development of drugs targeting oncogenic RAS.

The interaction between a biotinylated and farnesylated KRAS4B peptide[12] with His-tagged PDEδ was used in an high-throughput Alpha Screen (Supplementary Fig. 1) to identify small molecules that bind to the farnesyl-binding pocket of PDEδ. The screen yielded several benzimidazole hits (for example, **1**, Fig. 1a) which were further characterized by means of a fluorescence polarization assay based on a known PDEδ ligand[13] ($K_D = 165 \pm 23$ nM for compound **1**), isothermal titration calorimetry ($K_D = 217 \pm 15$ nM for **1**) and change in protein melting temperature upon interaction (see Supplementary Figs 2, 3 and 4)[14].

Crystal structure analysis of **1** in complex with PDEδ at 1.87 Å resolution (Fig. 1b and Supplementary Fig. 5) and comparison with the previously obtained structure of the complex between PDEδ and farnesylated RHEB (root mean squared deviation (r.m.s.d.) of 0.9 Å), revealed that two benzimidazoles bind into the hydrophobic tunnel in PDEδ (Fig. 1b). One molecule is deeply buried and overlaps with the farnesyl-binding site. The second molecule is located in the vicinity of the binding site that makes main chain contacts with two carboxy-terminal RHEB amino acids. Binding of the inhibitors is mediated by hydrophobic interactions and hydrogen bonding between the benzimidazole units and Tyr 149 and Arg 61 (Fig. 1b). Consistently, related N-benzylated 2-phenylindole shows no binding (Supplementary Fig. 3). Furthermore, the side chain of Trp 90 underwent a conformational change resulting in a T stacking with inhibitor **1** (Supplementary Fig. 6).

Structure-guided design based on the crystal structure obtained for **1** in complex with PDEδ suggested covalent linking of the benzimidazoles

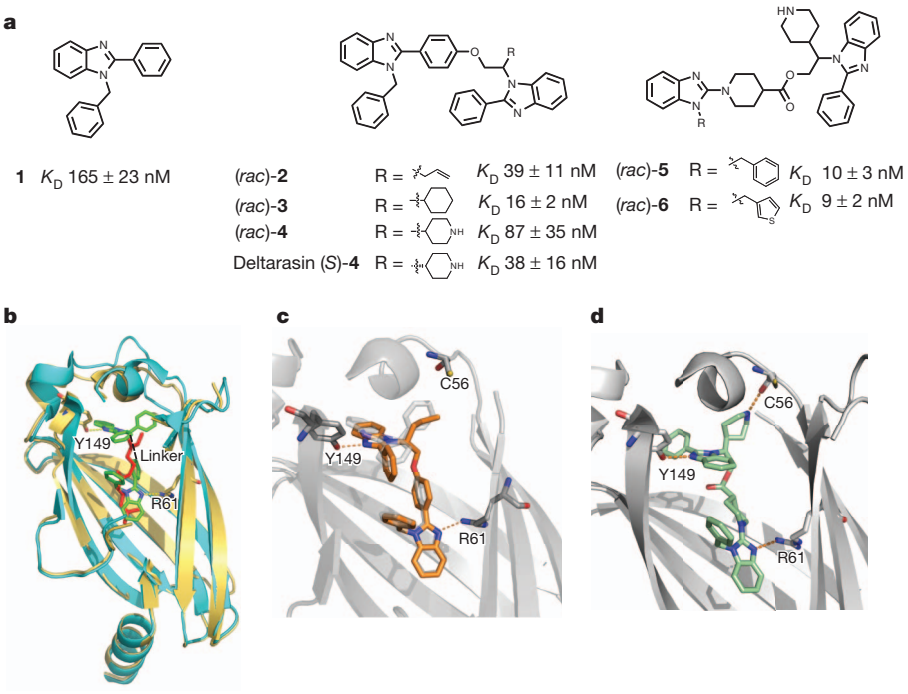

Figure 1 | Structure-based development of inhibitors. **a**, Structure and binding affinities of benzimidazole compounds **1**–**6** as determined by competitive fluorescence polarization assay (see Supplementary Information, Supplementary Fig. 3). **b**, Ribbon diagram of PDEδ structure in complex with **1** (yellow), and overlay with the previously obtained crystal structure of farnesylated RHEB peptide with PDEδ (cyan). Small molecule **1** (green) and farnesyl group (red) are shown as ball and sticks. Hydrogen bonding interactions between two molecules of **1** and Tyr 149 and Arg 61 in the co-crystal structure are highlighted. **c**, Structure of **2** (orange sticks) in complex with PDEδ. Overlaid is the structure of two molecules of **1** (faint grey sticks) in complex with PDEδ. **d**, Crystal structure of (*S*)-**5** in complex with PDEδ confirms the presence of a hydrogen bond between the piperidine and the backbone carbonyl of Cys 56.

[1]Department of Chemical Biology, Max Planck Institute of Molecular Physiology, D-44227 Dortmund, Germany. [2]Department of Systemic Cell Biology, Max Planck Institute of Molecular Physiology, D-44227 Dortmund, Germany. [3]Structural Biology Group, Max Planck Institute for Molecular Physiology, D-44227 Dortmund, Germany. [4]Department of Molecular Gastrointestinal Oncology, Ruhr-University Bochum, D-44801 Bochum, Germany. [5]Chemical Biology, Faculty of Chemistry, TU Dortmund, D-44227 Dortmund, Germany.
*These authors contributed equally to this work.

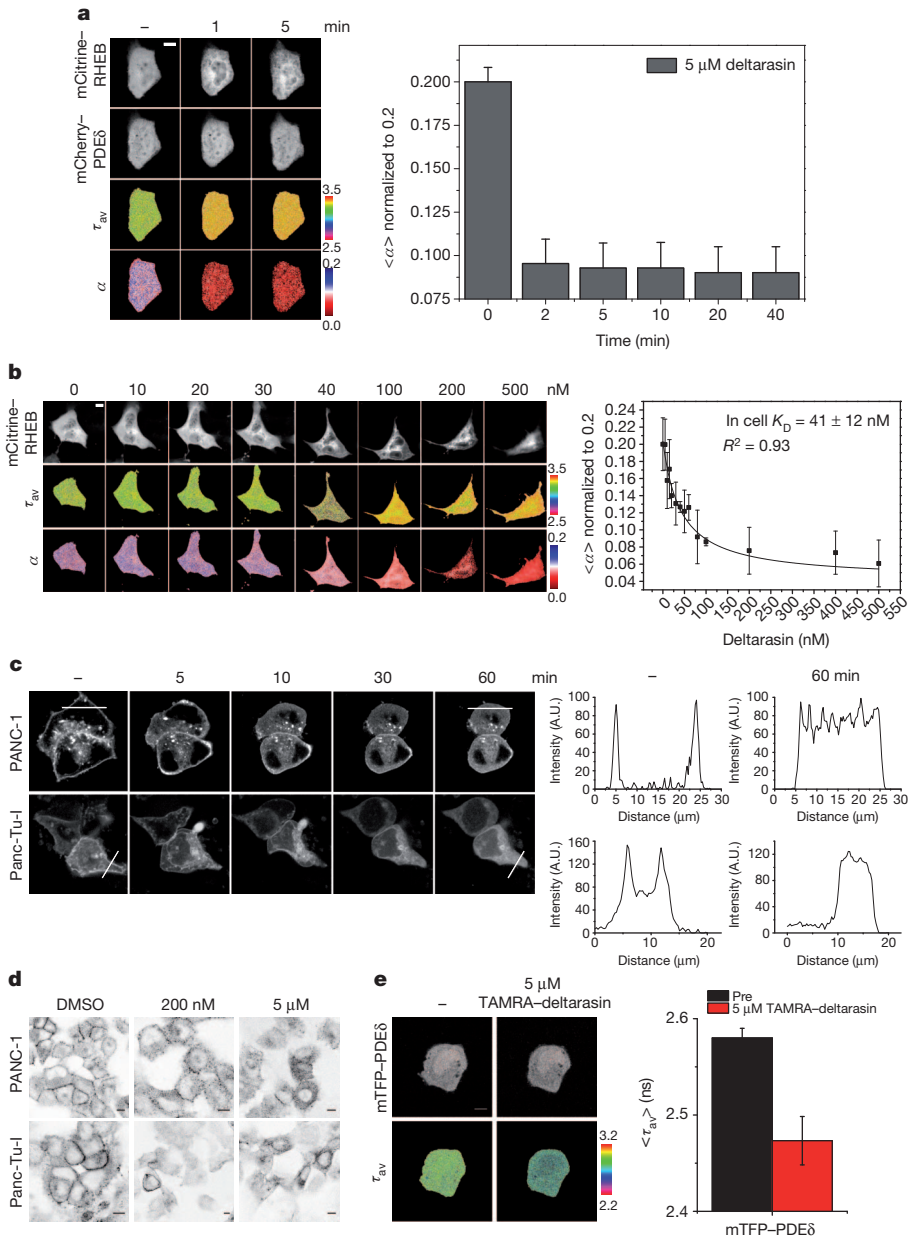

Figure 2 | In-cell measurements of the effect of deltarasin on the interaction of RAS with PDEδ and resulting delocalization of KRAS. **a**, FLIM time series on MDCK cells expressing mCitrine–RHEB and mCherry–PDEδ show a loss of interaction between RHEB and PDEδ after treatment with 5 μM deltarasin. Left panel, representative sample of FLIM time series. Upper two rows show fluorescence intensity distribution of the indicated fluorescent fusion proteins, whereas the lower two rows show maps of average fluorescence lifetime (τ_{av}) in ns and computed molar fraction (α) of interacting mCitrine–RHEB with mCherry–PDEδ. Time in minutes is indicated above the panels. The deltarasin-induced dissociation of mCherry–PDEδ and mCitrine–RHEB is represented in the time course of normalized average $<\alpha>$ ± s.e.m. for $N = 5$ cells in the right panel. **b**, Left panel, deltarasin dose dependence of molar fraction (α) of interacting mCitrine–RHEB with mCherry–PDEδ. Upper row shows fluorescence intensity distribution of mCitrine–RHEB, middle row shows average fluorescence lifetime (τ_{av}) in ns and lower row shows molar fraction (α) of interacting mCitrine–RHEB with mCherry–PDEδ. The concentration of deltarasin is indicated at the top of the panel in nM. Right panel, fit of averaged dose-response ± s.e.m. of four independent experiments to a binding model (see methods) yielded an in cell K_D of 41 ± 12 nM for deltarasin binding to PDEδ. **c**, Time series of mCitrine–KRAS redistribution upon application of 5 μM of deltarasin in PANC-1 (upper panel) and Panc-Tu-I (lower panel) cells. Time in minutes is indicated above the panel. The first and last time point of each cell line were used to quantify the mCitrine–KRAS distribution in these cells. The loss of plasma membrane localization can be seen in the mCitrine–KRAS intensity profiles along the white lines in the fluorescence micrographs in the right panels. A.U., arbitrary units. **d**, Immunofluorescence staining of fixed and permeabilized PDAC cells with a pan antibody against RAS (Calbiochem, Anti-Pan-RAS), 2 h after administration of the vehicle DMSO, 200 nM and 5 μM of deltarasin. **e**, FRET-FLIM measurements of the interaction between mTFP–PDEδ and TAMRA–deltarasin. Upper row, fluorescence intensity of mTFP–PDEδ; lower row, average fluorescence lifetime (τ_{av}) map of mTFP–PDEδ alone and in complex with the TAMRA–deltarasin. The averaged drop in the fluorescence lifetime ($<\tau_{av}>$ ± s.d.) of mTFP–PDEδ due to FRET with TAMRA–deltarasin is presented in the bar graph at the right side for $N = 3$ in each condition. Scale bars in all micrographs indicate 10 μm.

and synthesis of a focused library (Fig. 1a) with variation of the linker structure (see the Supplementary Information). Covalent linkage via an ether bond for instance yielded dimeric compound **2** (Fig. 1a), which binds to PDEδ with significantly increased affinity ($K_D = 39 \pm 11$ nM) and with an almost complete overlap with the positions of the individual benzimidazoles (Fig. 1c).

Investigation of the crystal structure of the complex (Fig. 1c) indicated replacement of the allyl group at R for a larger cyclohexyl moiety, which led to increased affinity (**3**, $K_D = 16 \pm 2$ nM, Fig. 1a), whereas introduction of a negative charge (R = CH_2COOH, $K_D = 870 \pm 290$ nM, see also Supplementary Table 1), omission of a substituent (R = H, $K_D = 116 \pm 29$ nM) or increased steric bulk (R = Boc(4-piperidine), $K_D > 2000$ nM), yielded less potent ligands.

The proximity of the backbone carbonyl of Cys 56 to substituent R (Fig. 1c) suggested introduction of a piperidine to introduce an additional hydrogen bond (Fig. 1c). However, piperidine-containing compound **4** (Fig. 1a) had lower affinity compared to **3**, probably due to rigidity of the linker that might not allow for three hydrogen-bonding interactions.

Replacement of the phenyl ether by a flexible piperidine 4-carboxylic acid ester resulted in an improvement of K_D by almost one order of magnitude (**5**, $K_D = 10 \pm 3$ nM, Fig. 1a). Crystal structure analysis of **5** in complex with PDEδ confirmed the presence of a hydrogen bond between the piperidine moiety in **5** and the carbonyl backbone of Cys 56 (Fig. 1d). Replacement of the benzyl moiety with a 3-methyl thiophene lead to a similarly potent compound (**6**, $K_D = 9 \pm 2$ nM, Fig. 1a).

Separation of the enantiomers of Boc-protected **4** and **6** by preparative chiral high-performance liquid chromatography (Supplementary Fig. 7), removal of the Boc group and biochemical investigation of the

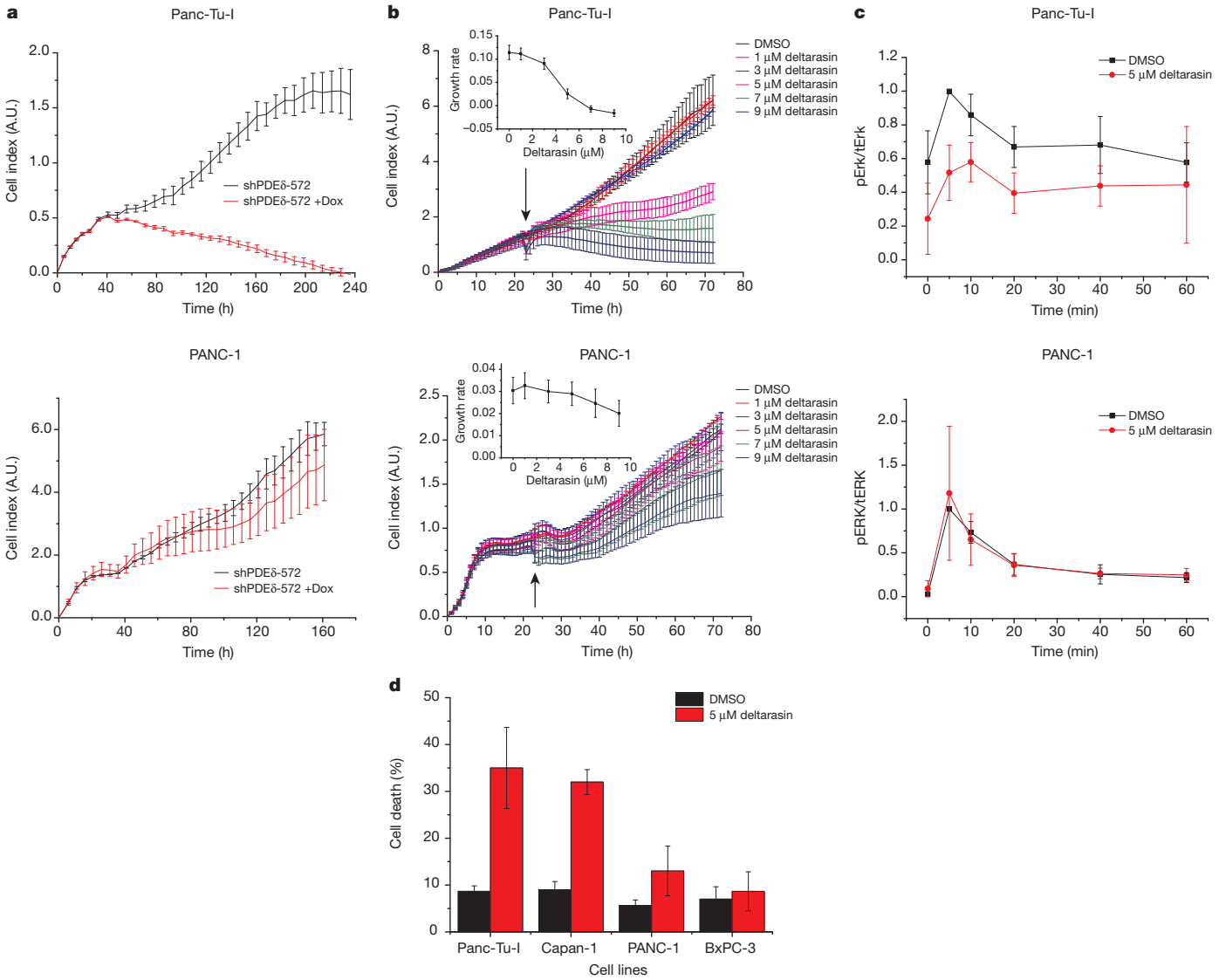

Figure 3 | Inhibition of PDEδ–KRAS interaction suppresses proliferation and MAPK-signalling in oncogenic KRAS-dependent PDAC cells. **a**, Real-time cell analysis (RTCA) of oncogenic KRAS-dependent Panc-Tu-I (upper panel) and oncogenic RAS-independent PANC-1 (lower panel) PDAC cell proliferation after doxycycline-induced PDEδ knock-down. Cells were transduced with shPDEδ-572 doxycycline-inducible knockdown vector. Cell indices ± s.d. were measured in duplicates. Cells were treated with doxycycline to induce PDEδ knockdown from the beginning of the experiment (+ Dox). **b**, RTCA of deltarasin dose PDAC cell proliferation response ± s.d. of oncogenic KRAS-dependent (Panc-Tu-I, upper panel) and KRAS-independent (PANC-1, lower panel) cell lines shows deltarasin-induced suppression of proliferation in oncogenic KRAS-dependent Panc-Tu-I cells. Deltarasin was added at the indicated time point (arrow) and concentration (1–9 μM). The inset in each panel shows deltarasin dose versus growth-rate response ± s.d. as determined from the average of the first derivative of the cell growth curves determined between 35 and 65 h (Supplementary Fig. 15). **c**, EGF-induced MAPK signalling response in PDAC cells treated with deltarasin. Peak normalized Erk1/Erk2 phosphorylation time profiles upon stimulation with 200 ng ml^{-1} EGF in serum starved Panc-Tu-I and PANC-1 cells as quantified from three independent western blots for each cell line. Each western blot contained the Erk1/Erk2 time response with vehicle control and deltarasin (Supplementary Fig. 18). The average ±s.d. is shown for each time point. Black, vehicle control DMSO; red, 2-h incubation with 5 μM deltarasin before EGF administration. **d**, Deltarasin induces cell death in KRAS-dependent PDAC cells (Panc-Tu-I, Capan-1) as measured by an annexin-V/propidium iodide FACS analysis (Supplementary Fig. 16). The bar graph shows the average ±s.d. of three independent experiments for each cell line and condition. Cells were analysed by FACS after 24 h of vehicle DMSO (black) and 5 μM deltarasin incubation (red).

pure enantiomers revealed a four to sixfold difference in potency for each pair of enantiomers ((*S*)-**4** $K_D = 38 \pm 16$ nM vs (*R*)-**4** $K_D = 190 \pm 55$ nM), and ((*S*)-**6** $K_D = 7 \pm 3$ nM vs (*R*)-**6** $K_D = 39 \pm 18$ nM. The absolute configuration was assigned by analogy to a previously reported synthesis (see the Supplementary Information)[15]. Tight binding of (*S*)-**4** and (*S*)-**6** to PDEδ was verified by means of a direct titration using 5-carboxytetramethyl rhodamine (TAMRA)-labelled (*S*)-**4** ($K_D = 7.6 \pm 1.3$ nM) and TAMRA–(*S*)-**6** ($K_D = 5.3 \pm 1.5$ nM, Supplementary Fig. 8). TAMRA–(*S*)-**4** and TAMRA–(*S*)-**6** did not bind to the PDEδ-homologous GDI-like solubilizing factors HRG4/Unc119a and Unc119b[16,17], nor to the presumed prenyl-binding proteins galectin-1 and galectin-3 (refs 18–20), indicating specificity for PDEδ (Supplementary Fig. 9). Compound **4** contains a hydrolytically stable ether linker (as opposed to an ester in **6**) and has appreciable solubility and membrane permeability (Supplementary Information), (*S*)-**4** was therefore used in the following cell biological studies. We term this compound deltarasin.

Fluorescence lifetime imaging microscopy (FLIM)-based fluorescence resonance energy transfer (FRET) measurements[21] were used to address whether deltarasin affected the interaction of PDEδ with

KRAS in live cells. To this end, mCherry–PDEδ was expressed together with mCitrine-tagged farnesylated RAS variants (KRAS6Q mutant or the RAS family protein RHEB) that lack part of the polybasic plasma membrane interaction motif of KRAS. Thus, their soluble fraction and interaction with PDEδ are strongly enhanced[9]. This largely facilitates the detection of the effect of small molecules on the interaction between mCitrine-tagged farnesylated RAS and mCherry–PDEδ in the cytoplasm of live cells by FLIM. The fluorescence patterns of mCitrine–RHEB or mCitrine–KRAS6Q and mCherry–PDEδ in Madine–Darby canine kidney (MDCK) cells transiently co-transfected with these proteins were homogeneous, showing a clear solubilization of mCitrine–RHEB/KRAS6Q by mCherry–PDEδ. A substantial drop in the mCitrine fluorescence lifetime showed that FRET occurred between the fluorescent proteins and corroborated that the solubilization of RHEB/KRAS6Q was due to a direct interaction with PDEδ (Fig. 2a and Supplementary Fig. 10). Computation of the fraction of interacting molecules (α) by global analysis of the fluorescence decay profiles as obtained by FLIM[21–23] showed that a significant fraction of mCitrine–RHEB/KRAS6Q was in complex with mCherry–PDEδ. Within a minute, 5 μM of deltarasin completely inhibited this interaction and released the insolubilized mCitrine–RHEB/KRAS6Q to the endomembrane system (Fig. 2a and Supplementary Fig. 10). This shows that deltarasin interferes with the binding of KRAS to PDEδ in cells and thereby inhibits its solubilization. Quantification of the interaction between mCherry–PDEδ and mCitrine–RHEB (or mCitrine–KRAS6Q) in live cells by global analysis of FLIM data as function of deltarasin dose (Fig. 2b and Supplementary Fig. 11) enabled the computation of an 'in cell' K_D of 41 ± 12 nM (27 ± 7 nM for the mCitrine–KRAS6Q assay) for the PDEδ–deltarasin interaction, remarkably similar to that determined for binding of deltarasin to purified PDEδ (38 ± 16 nM).

By analogy to PDEδ knockdown[9], treatment of human pancreatic ductal adenocarcinoma (PDAC) cell models PANC-1 and Panc-Tu-I with 5 μM deltarasin led within 1 h to a clear loss of mCitrine–KRAS (ectopically expressed) plasma membrane localization and its redistribution to endomembranes (Fig. 2c). Immunofluorescence staining of this type of PDAC cells with an anti-RAS antibody also showed that deltarasin induced a random distribution of endogenous RAS to endomembranes (Fig. 2d). Direct binding of deltarasin to PDEδ in live PANC-1 cells could also be demonstrated by the occurrence of FRET between monomeric teal fluorescent protein-tagged PDEδ (mTFP–PDEδ) and TAMRA-tagged deltarasin, as seen by the significant reduction in fluorescence lifetime of mTFP in the presence of TAMRA–deltarasin (Fig. 2e). These experiments show that inhibition of the PDEδ–KRAS interaction by binding of deltarasin to PDEδ leads to a loss of KRAS spatial organization in PDAC cells, as maintained by the solubilizing activity of PDEδ[9].

To assess the effect of deltarasin on oncogenic KRAS signalling, the growth of PDAC cells that are dependent on oncogenic KRAS for their survival (Panc-Tu-I and Capan-1 cells) was compared to PDAC cells that are independent of oncogenic KRAS (PANC-1 cells)[24] or express wild-type KRAS (BxPC-3 cells)[25]. Transfection of these PDAC cells with a lentiviral construct for doxycycline-inducible short hairpin RNA (shRNA) expression against PDEδ (Supplementary Figs 12 and 13) and treatment with doxycycline resulted in strongly reduced cell proliferation and cell death of the KRAS-dependent Panc-Tu-I and Capan-1 PDAC cell lines after 2–4 days and had only a slight effect on the growth of the other cell lines (Fig. 3a and Supplementary Fig. 14a). A similar effect on the proliferation of KRAS-dependent PDAC cells was found with the PDEδ inhibitor deltarasin (Fig. 3b and Supplementary Fig. 14b). The PDAC proliferation profiles as function of deltarasin dose (1–9 μM) show that the KRAS-dependent Panc-Tu-I cells show strongly reduced proliferation and increased cell death at around 5 μM deltarasin, whereas KRAS-independent PANC-1 cells only have a small negative dependence of growth rate on deltarasin concentration (Fig. 3b, d and Supplementary Figs 15 and 16). The KRAS-dependent Capan-1 cells also showed strongly reduced proliferation and increased cell death within hours upon treatment with 5 μM deltarasin, whereas the wild-type KRAS-harbouring BxPC-3 PDAC cells only had a slightly reduced initial growth rate and little or no increase in cell death with respect to the control (Fig. 3d and Supplementary Figs 14 and 16). These experiments indicate that the reduced proliferation of KRAS-dependent PDAC cells is caused in part by attenuated survival signalling from oncogenic KRAS that is delocalized on endomembranes. The deltarasin concentration (~3 μM, Fig. 3b) that induced a measurable effect on the proliferation of Panc-Tu-I cells was higher than that of complete inhibition of the interaction between PDEδ and RAS (~200 nM, Fig. 2b). Because deltarasin was found to be stable to metabolism by PDAC cells (Supplementary Fig. 17), this is probably due to the activity of ABC-transporters[26] that oppose the inward flux of the compound and thereby lower its intracellular availability at longer times.

To address whether KRAS relocalization by deltarasin-mediated PDEδ inhibition has an effect on oncogenic KRAS signal transduction by uncoupling it from its effectors at the plasma membrane[9], the epidermal growth factor (EGF)-induced mitogen-activated protein kinase (MAPK) response in serum-starved PDAC cells was studied. Quantitative western blot analysis of the phosphorylated Erk1 and Erk2 MAPKs showed that the KRAS-dependent Panc-Tu-I cells had a high basal Erk activity that was reduced upon inhibition of PDEδ by deltarasin (Fig. 3c and Supplementary Fig. 18). Strikingly, the two oncogenic KRAS-dependent PDAC cell lines (Panc-Tu-I and Capan-1) showed a substantial reduction in the EGF-mediated transient MAPK signal response as compared to the other cell lines (Fig. 3c and Supplementary Figs 14 and 18). The residual transient MAPK response to EGF can probably be attributed to the remaining wild-type RAS isoforms at the plasma membrane that are encoded by the healthy (wild-type) alleles. Therefore, oncogenic KRAS-dependent proliferative and survival signalling is strongly attenuated by the loss of KRAS plasma membrane localization as caused by the inhibition of PDEδ–KRAS interaction by deltarasin.

To evaluate the anti-tumour activity of deltarasin, we administered the compound to nude mice bearing subcutaneous human Panc-Tu-I tumour cell xenografts and monitored tumour growth rate. Deltarasin was administered by intra-peritoneal (i.p.) injection once (QD) or twice (BID) per day. Three dosage regiments were tested (10 mg kg^{-1} QD, 15 mg kg^{-1} QD and 10 mg kg^{-1} BID). An initial ~15% maximal weight loss of mice injected with deltarasin could be observed during the first 2 days of treatment, after which this stabilized in all groups (Supplementary Fig. 19). A clear dose-dependent reduction in Panc-Tu-I

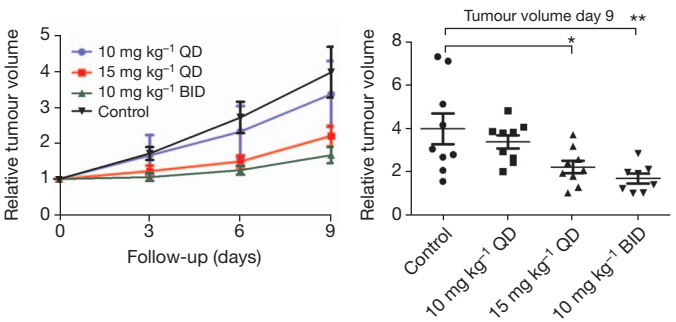

Figure 4 | Deltarasin impairs dose-dependent *in vivo* growth of xenografted pancreatic carcinoma in nude mice. **a**, **b**, Tumour volume measurements (**a**) and tumour volume distribution (**b**) at day 9 of Panc-Tu-I xenograft tumours treated with vehicle or deltarasin at the dosages indicated: deltarasin was administered by intra-peritoneal injection once (QD) or twice (BID) per day at 10 mg kg^{-1} QD, 15 mg kg^{-1} QD and 10 mg kg^{-1} BID. Changes in mean tumour volumes are given relative to the volumes at treatment initiation. Error bars represent s.e.m. with $n = 9$ for the control, 10 mg kg^{-1} QD, and 15 mg kg^{-1} QD and $n = 8$ for the 10 mg kg^{-1} BID group. P values were obtained by unpaired t-test. $^{**}P \leq 0.01$, $^{*}P \leq 0.05$.

tumour growth rate could be observed in deltarasin treated mice with respect to the vehicle-injected controls, where the growth of tumours in mice that were treated with 10 mg kg^{-1} BID deltarasin was almost completely blocked (Fig. 4a). The negative effect of the compound on Panc-Tu-I tumour growth could also be observed in the reduced variance in tumour size with respect to the control as measured at day 9 (Fig. 4b).

Our results demonstrate that inhibition of the PDEδ–KRAS interaction by means of small molecules affects the spatial organization of KRAS and thus provides a novel opportunity to suppress oncogenic RAS signalling and thereby tumour growth.

METHODS SUMMARY

Screening based on Alpha-technology was conducted in white, non-binding 1,536-well plates in a final volume of 6 µl (His_6–PDEδ, 100 nM, biotinylated KRAS peptide 250 nM).

K_D values were measured by fluorescence polarization measurements. For direct titrations, increasing amounts of PDEδ were added to a solution containing 50–100 nM labelled small molecule in 200 µl PBS buffer. For displacement titrations, increasing amounts of the small molecules in DMSO were directly added to fluorescein-labelled atorvastatin (24 nM) and His_6-tagged PDEδ (40 nM) in 200 µl PBS-buffer (containing 0.05% CHAPS, 1% DMSO), keeping the concentration of fluorescein-labelled atorvastatin, PDEδ and DMSO constant.

For K_D measurements using isothermal titration calorimetry, PDEδ protein (280 µM) was titrated to small molecule (30 µM) in Tris/HCl buffer (temperature 25 °C). In the T_m shift assays, protein melting points were detected by circular dichroism spectroscopy in the presence of small molecules.

Inhibitors were co-crystallized with PDEδ by mixing a solution of small molecule and PDEδ with DMSO 1.7% as a final concentration. Crystals were obtained from a Qiagen crystallization screen.

For live-cell microscopy, cells were grown in four-well Lab-Tek chambers (NUNC) and transferred to low-bicarbonate DMEM without phenol red supplemented with 25 mM HEPES at pH 7.4.

The following antibodies were used for western blotting: total Erk (Abcam-AB36991; 1:2,000), pErk (Cell Signaling-9101; 1:2,000) and infrared secondary antibodies (LI-COR).

Fluorescence lifetime images were acquired using a confocal laser-scanning microscope (FV1000, Olympus) equipped with a time-correlated single-photon counting module (LSM Upgrade Kit, Picoquant). Intensity thresholds were applied to segment the cells from the background fluorescence. Data were further analysed as described in ref. 23 to obtain images of the molar fraction (α) of interacting mCherry–PDEδ/mCitrine–RHEB.

Real-time cell analyses were carried out by monitoring the proliferation for at least 3 days after administration of the inhibitor.

Received 23 August 2012; accepted 19 April 2013.
Published online 22 May 2013.

1. Malumbres, M. & Barbacid, M. *RAS* oncogenes: the first 30 years. *Nature Rev. Cancer* **3,** 459–465 (2003).
2. Gelb, M. H. *et al.* Therapeutic intervention based on protein prenylation and associated modifications. *Nature Chem. Biol.* **2,** 518–528 (2006).
3. Downward, J. Targeting RAS signalling pathways in cancer therapy. *Nature Rev. Cancer* **3,** 11–22 (2003).
4. Berndt, N., Hamilton, A. D. & Sebti, S. M. Targeting protein prenylation for cancer therapy. *Nature Rev. Cancer* **11,** 775–791 (2011).
5. Roberts, P. J. & Der, C. J. Targeting the Raf-MEK-ERK mitogen-activated protein kinase cascade for the treatment of cancer. *Oncogene* **26,** 3291–3310 (2007).
6. Maurer, T. *et al.* Small-molecule ligands bind to a distinct pocket in Ras and inhibit SOS-mediated nucleotide exchange activity. *Proc. Natl Acad. Sci. USA* **109,** 5299–5304 (2012).
7. Patgiri, A., Yadav, K. K., Arora, P. S. & Bar-Sagi, D. An orthosteric inhibitor of the Ras-Sos interaction. *Nature Chem. Biol.* **7,** 585–587 (2011).
8. Sun, Q. *et al.* Discovery of small molecules that bind to K-Ras and inhibit Sos-mediated activation. *Angew. Chem. Int. Edn* **51,** 6140–6143 (2012).
9. Chandra, A. *et al.* The GDI-like solubilizing factor PDEδ sustains the spatial organization and signalling of Ras family proteins. *Nature Cell Biol.* **14,** 329–329 (2012).
10. Ismail, S. A. *et al.* Arl2-GTP and Arl3-GTP regulate a GDI-like transport system for farnesylated cargo. *Nature Chem. Biol.* **7,** 942–949 (2011).
11. Zhang, H. *et al.* Photoreceptor cGMP phosphodiesterase δ subunit (PDEδ) functions as a prenyl-binding protein. *J. Biol. Chem.* **279,** 407–413 (2004).
12. Chen, Y. X. *et al.* Synthesis of the Rheb and K-Ras4B GTPases. *Angew. Chem. Int. Edn* **49,** 6090–6095 (2010).
13. Chidley, C., Haruki, H., Pedersen, M. G., Muller, E. & Johnsson, K. A yeast-based screen reveals that sulfasalazine inhibits tetrahydrobiopterin biosynthesis. *Nature Chem. Biol.* **7,** 375–383 (2011).
14. Vedadi, M. *et al.* Chemical screening methods to identify ligands that promote protein stability, protein crystallization, and structure determination. *Proc. Natl Acad. Sci. USA* **103,** 15835–15840 (2006).
15. Monovich, L. G. *et al.* Discovery of potent, selective, and orally active carboxylic acid based inhibitors of matrix metalloproteinase-13. *J. Med. Chem.* **52,** 3523–3538 (2009).
16. Wright, K. J. *et al.* An ARL3–UNC119–RP2 GTPase cycle targets myristoylated NPHP3 to the primary cilium. *Genes Dev.* **25,** 2347–2360 (2011).
17. Zhang, H. *et al.* UNC119 is required for G protein trafficking in sensory neurons. *Nature Neurosci.* **14,** 874–880 (2011).
18. Elad-Sfadia, G., Haklai, R., Balan, E. & Kloog, Y. Galectin-3 augments K-Ras activation and triggers a Ras signal that attenuates ERK but not phosphoinositide 3-kinase activity. *J. Biol. Chem.* **279,** 34922–34930 (2004).
19. Paz, A., Haklai, R., Elad-Sfadia, G., Ballan, E. & Kloog, Y. Galectin-1 binds oncogenic H-Ras to mediate Ras membrane anchorage and cell transformation. *Oncogene* **20,** 7486–7493 (2001).
20. Bhagatji, P., Leventis, R., Rich, R., Lin, C. J. & Silvius, J. R. Multiple cellular proteins modulate the dynamics of K-ras association with the plasma membrane. *Biophys. J.* **99,** 3327–3335 (2010).
21. Wouters, F. S., Verveer, P. J. & Bastiaens, P. I. H. Imaging biochemistry inside cells. *Trends Cell Biol.* **11,** 203–211 (2001).
22. Grecco, H. E. *et al. In situ* analysis of tyrosine phosphorylation networks by FLIM on cell arrays. *Nature Methods* **7,** 467–472 (2010).
23. Grecco, H. E., Roda-Navarro, P. & Verveer, P. J. Global analysis of time correlated single photon counting FRET-FLIM data. *Opt. Express* **17,** 6493–6508 (2009).
24. Moore, P. S. *et al.* Genetic profile of 22 pancreatic carcinoma cell lines. *Virchows Arch.* **439,** 798–802 (2001).
25. Berrozpe, G., Schaeffer, J., Peinado, M. A., Real, F. X. & Perucho, M. Comparative-analysis of mutations in the *p53* and K-*ras* genes in pancreatic-cancer. *Int. J. Cancer* **58,** 185–191 (1994).
26. Perez-Tomas, R. Multidrug resistance: retrospect and prospects in anti-cancer drug treatment. *Curr. Med. Chem.* **13,** 1859–1876 (2006).

Supplementary Information is available in the online version of the paper.

Acknowledgements The research leading to these results has received funding from the European Research Council under the European Union's Seventh Framework Program (FP7/2007-2013)/ERC Grant agreement no. 268309 to H.W., and no. 268782 to A.W. The Compound Management und Screening Center (COMAS), Dortmund, Germany, is acknowledged for carrying out high-throughput screening and data analysis. G.Z. acknowledges the Fonds der Chemischen Industrie for a Kekulé Scholarship. We thank K. Michel for help with western blot analysis. We are grateful to C. Degenhart, A. Wolf, S. Baumann and A. Choidas for help with screening assay development and for the determination of solubility, membrane permeability and stability of deltarasin.

Author Contributions A.W., P.I.H.B. and H.W. conceived the project. H.W., G.T. and G.Z. developed the screen and chemistry to generate the PDEδ inhibitor, P.I.H.B. designed the cell biological experiments and A.W. with S.I. solved the structures by X-ray crystallography. A.W., H.W., S.I. and G.Z. designed the PDEδ structure-based inhibitor development. S.A.H. developed the inducible shRNA systems and the xenograft model, G.Z. synthesized the inhibitors and performed the biochemical and biophysical characterization experiments, B.P. performed the real-time cell analysis, FACS and western blot analysis. N.V., B.P. and A.C. performed the microscopy experiments. M.H. performed the shRNA real-time cell analysis and xenograft experiments. H.W. and P.I.H.B. wrote the manuscript with help from A.W., S.I., B.P., G.T. and G.Z.

Author Information The atomic coordinates of PDEδ in complex with inhibitor **1**, *rac*-**S1**, *rac*-**2** and (*S*)-**5** are deposited in the Protein Data Bank with accession numbers 4JV6, 4JV8, 4JVB and 4JVF, respectively. Reprints and permissions information is available at www.nature.com/reprints. The authors declare competing financial interests: details are available in the online version of the paper. Readers are welcome to comment on the online version of the paper. Correspondence and requests for materials should be addressed to H.W. (herbert.waldmann@mpi-dortmund.mpg.de), P.I.H.B. (philippe.bastiaens@mpi-dortmund.mpg.de) or A.W. (alfred.wittinghofer@mpi-dortmund.mpg.de).